

A Fault Location Scheme for Active Untransposed Distribution Systems Using a Limited Number of Synchronized Measurements

Fathy Aboshady^{1,2,*}, David Thomas¹ and Mark Sumner¹

¹Department of Electrical and Electronic Engineering, University of Nottingham, Nottingham, UK

²Electrical Power and Machines Engineering Department, Tanta University, Tanta, Egypt

Abstract This paper presents a fault location scheme for unbalanced and untransposed distribution systems which contain different types of distributed generation (DG). A general formula has been derived for any fault type using a limited number of synchronized measurement points. To avoid having to synchronize all of the measurement points, the voltage and current measured locally at the DGs are processed locally to calculate the equivalent impedance of the DG at the non-fundamental frequencies. This is then used in the fault location process. The IEEE 34-bus feeder is simulated using the distributed parameter model for the lines and is used to validate the proposed scheme. Uncertainties associated with fault type, fault location, fault resistance, inception angle, noise in measurements and load profile are considered in the evaluation. The simulation studies demonstrate that the scheme can have a high accuracy and is robust.

Keywords: distributed generation; distribution systems; fault location; fault transient; impedance based

1 Introduction

The distribution system is experiencing a change in nature with the increasing penetration of distributed generation (DG). Power flow and fault characteristics are among the factors that will be affected by the integration of these devices and the way they are affected depends on the characteristics of the DG [1]. DGs can be of different types, however, climate change, global warming and other environmental issues are driving the integration of renewable energy sources such as solar energy and wind energy to replace conventional generation systems [2]. Therefore, studies are currently being conducted to keep pace with the features of future distribution system from different points of view including protection and fault location [3], [4].

Fault location studies aim to accurately identify the faulty part of the network so it could be fixed and restored as quickly as possible [3]. Research in fault location considers different methodologies. In brief, impedance based methods employ the measured voltages and currents to estimate the impedance to the fault and transform it to a distance using the line's

per-unit length parameters [5]–[11]. With Travelling Wave based methods, the high frequency wave generated when a fault occurs is captured and used to calculate the wave travelling time between the fault point and the measurement point(s). The fault distance is then estimated based on the travelling time and speed of propagation [12], [13]. Computational Intelligence based methods such as artificial neural networks are trained with different fault scenarios and conditions and are then used to identify the fault point [14], [15]. Methods based on voltage sag compare the measured voltage from different locations in the network and the estimated voltages from a network model which simulates the fault at different nodes. The node with the highest matching factor is deemed to be the fault point [16].

Impedance based methods have a relatively low implementation cost and can be very accurate but suffer from the fact that many points may have the same electrical impedance value to the measurement point [3]. This problem is known as the “multiple estimation problem”. However, they can be integrated with other methods to overcome this shortfall [17]. Some of the recent impedance based methods that have been developed for active distribution systems, have been reported in [5]–[10]. These methods can be classified based on the number and type of measurement points. In [5]–[7], synchronized measurements from the main substation and the DG units were used. Non-synchronized measurements were used in [8]. The error in the synchronization angle is considered as unknown and can be calculated using an iterative load flow algorithm. In [9], [10], only the measurements at the main substation were used. However, a model for the DG is necessary to apply these methods. The DG model changes based on the DG type and its characteristics. Also, detailed DG knowledge of the parameters may be necessary to build the model. A simple synchronous based distributed generation (SBDG) unit represented as a source behind an impedance has been considered in [10], whereas an inverter based distributed generation (IBDG) unit has been modelled in [9]. The model developed depends on the DG operating mode during the fault, and this operating mode depends on the fault

*Corresponding author

current level. In [9], the DG current is estimated using a ladder iterative technique.

This paper presents an impedance based fault location scheme based on system analysis using the non-fundamental high frequency components generated when a fault occurs. The proposed scheme uses the available synchronized and non-synchronized measurements in the system to locate the fault point. The paper presents the following contributions to the research literature:

1. The proposed scheme eliminates the need for using synchronized measurements from all generation units.
2. It does not require the synchronization of the non-synchronized measurements, which is the problem with impedance based fault location methods that use non-synchronized measurements.
3. The parameters of the distributed generators are not required in order to apply the method.
4. The method is applicable to unbalanced distribution networks with untransposed lines and is derived and verified using the distributed parameter line model.
5. The method uses a short window of data captured during the fault (only one cycle). Therefore, it can locate intermittent faults as well as permanent faults.

2 Proposed Methodology

As stated in the introduction, the distributed generation is considered in fault location methods by either using synchronized measurements from all DGs, using non-synchronized measurements and solving for the synchronization error or developing a DG model at the system fundamental frequency. The latter case requires a detailed knowledge of the DG parameters, type and operating conditions [18].

In this paper, measurements from different DG units are used to avoid the need for DG modelling. However, synchronized measurements from these different locations are not necessary. Also, solving for the synchronization error is not required. Firstly, the DG representation concept is illustrated and then the fault location formula is derived in the subsequent sections.

2.1 DG Representation

The proposed fault location scheme does not require synchronized measurements from all power sources (main substation and DGs) in the system. Instead, the voltage and current measurements available at each DG location are processed locally at the DG unit itself. The processing aims to find the DG equivalent impedance as seen from the point of its interconnection to the grid. Even though the DG is modelled as an active circuit at the system fundamental frequency,

the proposed method assumes the DG can be represented as an impedance (passive element) at higher (non-fundamental) frequencies. To illustrate this concept, consider a SBDG. The SBDG equivalent circuit at the system fundamental frequency is ideally a source behind an impedance as shown in Figure 1. Therefore, at the non-fundamental frequencies and according to the superposition theorem, the DG can be modelled as an impedance as shown in Figure 1 which matches the proposed assumption. For the IBDG, it is well known that inverters produce switching harmonics and some low order harmonics as well as the main frequency component. However, this type of DG is connected to the system through filters that are designed to reduce the effect of the non-fundamental frequency components to meet requirements from appropriate system standards [19]. Despite the IBDG is a non-linear system at the fundamental frequency, it has been experimentally proven in [20] that this DG can be approximated to a linear system at high frequency ranges.

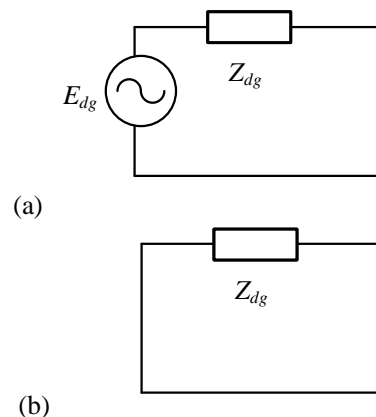


Figure 1: SBDG model (a) fundamental frequency (b) non-fundamental frequencies

The DG impedance at non-fundamental frequencies can be calculated locally at the DG unit. For this purpose, a data window that combines both pre-fault data and data captured during the fault are used and the Fast Fourier Transform (FFT) is employed to calculate the DG impedance over the frequency range of interest (1). A series of values for Z_{dg} at different frequencies is generated locally. It can then be transferred to the main substation to be used by the proposed fault location algorithm. Assuming that the voltage and current measurements at the DG unit are synchronized with each other but are not synchronized with those at the main substation, this will have little effect on the calculated impedance as the synchronization error in the voltage cancels that in the current and the ratio is maintained the same as (1). The cal-

culated impedance can be transferred to the main substation using an asynchronous channel. Alternatively, the non-synchronized voltage and current are sent to the main substation and processed to estimate the DG impedance at the (non-fundamental) higher frequency components.

$$Z_{dg} = FFT(V_{dg})/FFT(I_{dg}) \quad (1)$$

2.2 Method Derivation

From the previous subsection, DGs that do not have synchronized measurements with the main substation are represented by their calculated equivalent impedance in the fault location process. The proposed method then employs the available synchronized measurements to estimate the fault distance. In this study, the method is illustrated assuming the availability of two synchronized measurement points at the start and end nodes of the main feeder. The proposed method is based on analysing the system during the fault transient period using a data window for both voltage and current that contains both pre-fault data and data captured during the fault. The non-fundamental frequency components calculated using the FFT for this window are used to estimate the fault distance.

In order to generalize the analysis for different line configurations, the distributed parameter line model is used. Therefore, mutual inductance and capacitance, capacitance to ground, line asymmetry and untransposed lines are considered. For a three-phase system, the transformation between phase domain and mode domain is used to decouple the system into three independent propagation modes (ground mode and two aerial modes) [21].

$$\begin{aligned} V_{012} &= T_v^{-1} V_{abc} & I_{012} &= T_i^{-1} I_{abc} \\ z_{012} &= T_v^{-1} z_{abc} T_i & y_{012} &= T_i^{-1} y_{abc} T_v \end{aligned} \quad (2)$$

where (0, 1, 2) are the ground and the two aerial modes, (a, b, c) are the phase components, z is the line series impedance matrix, y is the line shunt admittance matrix, the transformation matrices T_v and T_i are the eigenvectors of $z_{abc}y_{abc}$ and $y_{abc}z_{abc}$ respectively. Also, the propagation constant γ and the characteristic impedance z_c of the line are given by (3), where j refers to the propagation mode.

$$\gamma_j = \sqrt{z_j y_j}, \quad z_{c_j} = \gamma_j^{-1} z_j \quad (3)$$

Consider a fault in an active distribution system as shown in Figure 2. The voltage and current at nodes S and R can be calculated from the available measurements and this will be explained later in the paper. The voltage at the fault point can be calculated based on the voltage and the current at both S and R by (4) and (5), where j refers to the propagation mode.

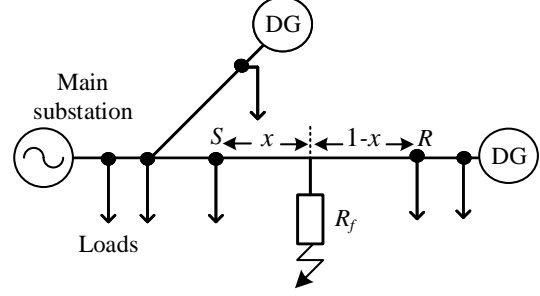


Figure 2: General active distribution system with a fault

$$V_{x_j} = \cosh(\gamma_j x) V_{S_j} - z_{c_j} \sinh(\gamma_j x) I_{S_j} \quad (4)$$

$$V_{x_j} = \cosh(\gamma_j (1-x)) V_{R_j} + z_{c_j} \sinh(\gamma_j (1-x)) I_{R_j} \quad (5)$$

Using the first two terms of the Taylor series for both cosh and sinh in (4) and (5), the third order polynomials in (6) and (7) are obtained.

$$V_{x_j} = A_{S_j} + B_{S_j} x + C_{S_j} x^2 + D_{S_j} x^3 \quad (6)$$

$$V_{x_j} = A_{R_j} + B_{R_j} x + C_{R_j} x^2 + D_{R_j} x^3 \quad (7)$$

where the values for the different constants are given in (8):

$$\begin{aligned} A_{S_j} &= V_{S_j} & B_{S_j} &= -\gamma_j z_{c_j} I_{S_j} \\ C_{S_j} &= \gamma_j^2 V_{S_j} / 2 & D_{S_j} &= -\gamma_j^3 z_{c_j} I_{S_j} / 6 \\ A_{R_j} &= V_{R_j} & B_{R_j} &= \gamma_j z_{c_j} I_{R_j} \\ C_{R_j} &= \gamma_j^2 V_{R_j} / 2 & D_{R_j} &= \gamma_j^3 z_{c_j} I_{R_j} / 6 \\ A_{R_j} &= A_{r_j} + B_{r_j} + C_{r_j} + D_{r_j} & C_{R_j} &= C_{r_j} + 3D_{r_j} \\ B_{R_j} &= -(B_{r_j} + 2C_{r_j} + 3D_{r_j}) & D_{R_j} &= -D_{r_j} \end{aligned} \quad (8)$$

The voltage V_x can be expressed in the phase domain by (9) and (10) using (2).

$$\begin{aligned} V_{x_{abc}} &= A_{S_{abc}} + B_{S_{abc}} x + C_{S_{abc}} x^2 + D_{S_{abc}} x^3 \\ &= [V_{xa} \ V_{xb} \ V_{xc}]^t \end{aligned} \quad (9)$$

$$V_{x_{abc}} = A_{R_{abc}} + B_{R_{abc}} x + C_{R_{abc}} x^2 + D_{R_{abc}} x^3 \quad (10)$$

where t refers to the non-conjugate transpose, $K_{abc} = T_v K_{012}$, K refers to $A_S, B_S, C_S, D_S, A_R, B_R, C_R, D_R$, $K_{abc} = [K_a \ K_b \ K_c]^t$, $K_{012} = [K_0 \ K_1 \ K_2]^t$. By equating (9) and (10), the fault distance can be calculated using (11).

$$\begin{aligned} (A_{S_{abc}} - A_{R_{abc}}) + (B_{S_{abc}} - B_{R_{abc}}) x + \\ (C_{S_{abc}} - C_{R_{abc}}) x^2 + (D_{S_{abc}} - D_{R_{abc}}) x^3 = 0 \end{aligned} \quad (11)$$

The formula in (11) represents three equations for the three phases. It is only solved for the faulted phase(s). For a phase fault e.g. a fault between phase a and phase b , the corresponding line to line voltage from (9) and (10) is used to generate a single equation instead of solving two equations separately for the two phases. The three roots are the possible solutions for (11). The correct root should be real positive and less than the fault section length. The distance x is estimated at many frequencies over a wideband of frequencies up to 3 kHz and the final fault distance is the average value for these estimates. The frequency components below 250 Hz have been ignored as they will not be accurate when using this short transient period and also to avoid any effect from the system fundamental frequency on the DG impedance calculation.

As shown in Figure 2, the distribution system consists of many sections. Firstly, the fault is assumed in the line section next to the main substation and the fault distance is estimated using (11). If the estimated distance is greater than the assumed section length, a new fault section is considered based on the estimated value and the process of distance estimation is applied to this new section. The most systematic way to do this is to sweep along the feeder's sections one by one. The flowchart in Figure 3 illustrates this iterative process. To apply (11), the voltage and current at the sending and receiving ends of the assumed fault section need to be estimated and this is described in Section 3.

Regarding the computational time required to determine the fault distance using the proposed method, it is important to clarify that it is not necessary to perform the fault location process in real time with distribution systems [17].

3 System Reduction

3.1 Measurement Sweep

For the assumed fault section, it is necessary to calculate the voltage and current at both section ends (nodes S and R in the method derivation). This can be achieved by recursively sweeping the measurements downstream or upstream based on the location of the fault section with respect to the measurement points. The following group of equations illustrates this measurement flow in the mode domain where (12) and (13) are used for the downstream sweep and (14) and (15) are used for the upstream sweep (refer to Figure 4).

$$\begin{bmatrix} V_{k+1_j} \\ I'_{k+1_j} \end{bmatrix} = \begin{bmatrix} \cosh(\gamma_j l) & -z_{c_j} \sinh(\gamma_j l) \\ -\sinh(\gamma_j l)/z_{c_j} & \cosh(\gamma_j l) \end{bmatrix} \begin{bmatrix} V_{k_j} \\ I_{k_j} \end{bmatrix} \quad (12)$$

$$I_{k+1_j} = I'_{k+1_j} - Y_{L(k+1)} V_{k+1_j} \quad (13)$$

$$\begin{bmatrix} V_{k_j} \\ I_{k_j} \end{bmatrix} = \begin{bmatrix} \cosh(\gamma_j l) & z_{c_j} \sinh(\gamma_j l) \\ \sinh(\gamma_j l)/z_{c_j} & \cosh(\gamma_j l) \end{bmatrix} \begin{bmatrix} V_{k+1_j} \\ I'_{k+1_j} \end{bmatrix} \quad (14)$$

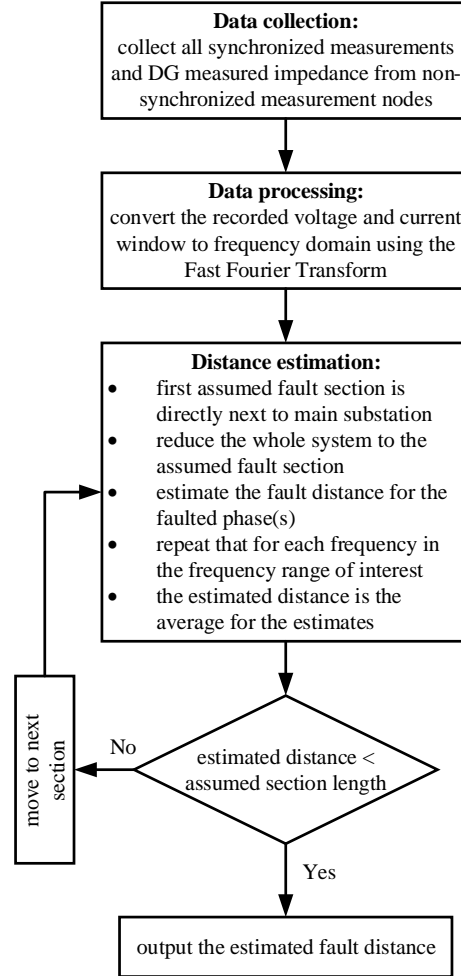


Figure 3: Procedure of the proposed method

$$I'_{k_j} = I_{k_j} + Y_{L(k)} V_{k_j} \quad (15)$$

where l is the length of the section between nodes k and $k + 1$, $Y_{L(k)}$ is the equivalent admittance at node k (and is illustrated in subsection 3.2).

3.2 Equivalent Impedance/Admittance

In the previous step, the equivalent admittance/impedance at different nodes is required. This admittance may be a load/DG admittance when a load/DG is directly connected at this node or the resultant value when a DG and a load are connected at the same node. However, when a lateral with multiple line sections and loads is connected at a certain node, the equivalent lateral impedance is calculated using a recursive procedure starting from the end node of the lateral. To illustrate this, consider the system in Figure 5, and the target is to calculate the equivalent impedance $Z_{eq(m)}$ starting with knowledge of the

downstream impedance $Z_{eq(m+1)}$. The relationship between the voltage and current at nodes m and $m+1$ is given by (16) and the relationship between the voltage and current at node $m+1$ is given by (17).

$$\begin{bmatrix} V_{m+1_j} \\ I_{m+1_j} \end{bmatrix} = \begin{bmatrix} A_{l_j} & B_{l_j} \\ C_{l_j} & D_{l_j} \end{bmatrix} \begin{bmatrix} V_{m_j} \\ I_{m_j} \end{bmatrix} \quad (16)$$

where $A_{l_j} = D_{l_j} = \cosh(\gamma_j l)$, $B_{l_j} = z_{c_j} \sinh(\gamma_j l)$ and $C_{l_j} = \sinh(\gamma_j l)/z_{c_j}$.

$$V_{m+1_j} = Z_{eq(m+1)_j} I'_{m+1_j} \quad (17)$$

Substituting (17) in to (16), the equivalent impedance $Z_{eq(m)}$ can be obtained as (18):

$$Z_{eq(m)_j} = [(C_{l_j} Z_{eq(m+1)_j} + D_{l_j})(A_{l_j} Z_{eq(m+1)_j} + B_{l_j})^{-1} + Y_{L(m)_j}]^{-1} \quad (18)$$

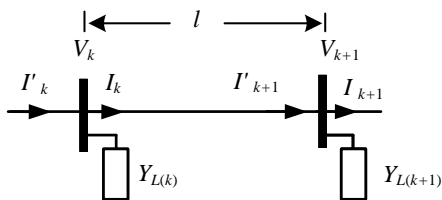


Figure 4: Sweep for measurements

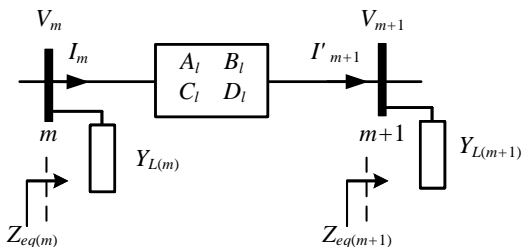


Figure 5: Equivalent impedance calculation

4 Simulation Studies

The IEEE 34-bus feeder was used to validate the proposed scheme for different test scenarios [22] (refer to Figure 6). It is a real medium voltage distribution feeder and contains unbalanced loads, non-homogeneous feeder sections, an asymmetrical line configuration and single and three-phase laterals. In the

simulation studies, the exact asymmetric line parameters as stated in [22] were used and the loads were assumed to be constant impedance loads. The system was modified by connecting three DGs of 250 kVA each. Two IBDGs were connected at nodes 848 and 840 and one SBDG was connected at node 828. A step up transformer was used to connect the DG to the main power grid. The parameters of the IBDG have been included in the Appendix. The DC side of the IBDG is connected to a DC source and a controller was used to follow the power reference. For the SBDG, a dynamic model for the synchronous machine from the Matlab/Simulink has been used. Although synchronized measurements were assumed between the main substation and the DG at node 848, non-synchronized measurements were used at the other DGs at nodes 840 and 828. For different evaluation scenarios, single line to ground (*ag*), line to line (*ab*) and three-phase (*abc*) faults were simulated at seven locations along the feeder. The error in estimating the fault distance is calculated as the absolute difference between the actual and the estimated distances (19).

$$error = |actual\ distance - estimated\ distance| \quad (19)$$

4.1 Effect of Fault Resistance

Fifty values of fault resistance between 0.01Ω and 100Ω (randomly generated) have been used to evaluate the performance of the proposed method. For each fault resistance value, the three fault types (*ag*, *ab* and *abc*) were simulated at seven locations. In this scenario, the fault inception angle is maintained at 90° . The error in the distance estimation at a distance of 16.85 km from the main substation is illustrated in Figure 7 and it can be seen that the error is less than 50 m. In total, 1050 fault cases were simulated for this scenario and the results are shown in Figure 8. The results show that all cases have an error of less than 60 m and the total average error is 17.2 m. Note that the number of points for certain locations and fault types in Figure 8 appears to be less than 50 as the error is the same value for different fault resistance values. Table 1 summarizes the results obtained where the percentage of the cases with an error of less than 50 m, the average (avg) and the maximum (max) error values are given for each fault type. These statistics reflect the accuracy of the proposed scheme for different fault resistances and different fault types.

4.2 Effect of Fault Inception Angle

The fault inception angle represents the voltage angle at the instant of the fault inception. The main substation source phase angle has been varied in this test to give 50 values randomly generated between 0° and 180° while keeping the fault resistance at 10Ω . Similar

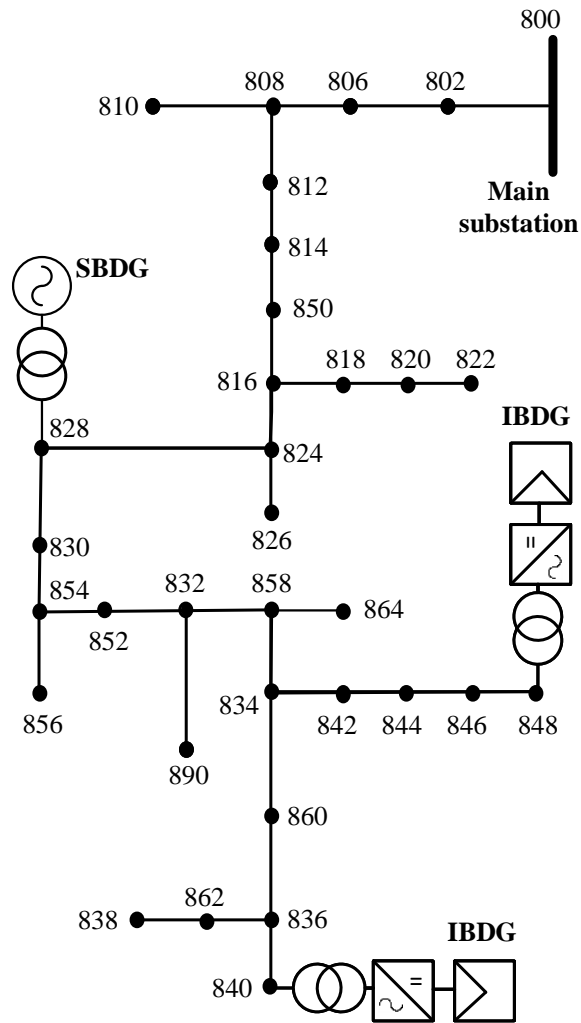


Figure 6: Single line diagram of the IEEE 34-bus feeder with DGs

to the previous test, different fault types were simulated at different locations. Figure 9 shows the error values obtained for these 1050 fault cases and Table 1 summarizes the results. With a total average error of 19.6 m and a maximum error of 121 m, it is clear that the proposed scheme provides an accurate estimation for different fault inception angles.

Table 1: Summary for fault resistance and inception angle tests

fault	fault resistance test			inception angle test		
	cases (%)	error (m)		cases (%)	error (m)	
		avg	max		avg	max
<i>ag</i>	100	11.7	48	95.4	16.4	83
<i>ab</i>	100	16.3	37	100	17.3	45
<i>abc</i>	98.8	23.7	51	86	25.1	121

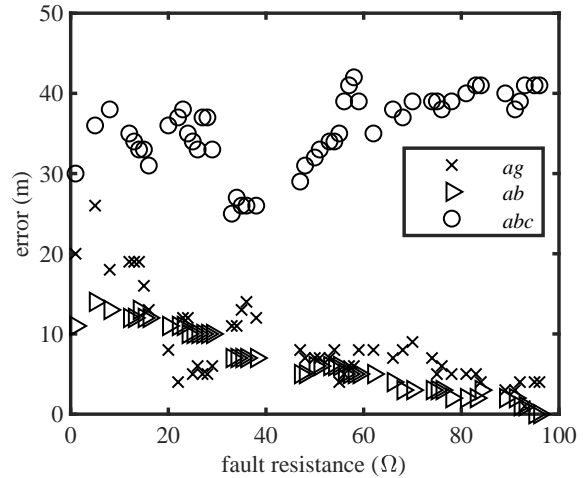


Figure 7: Error in distance estimation for faults at a distance of 16.85 km

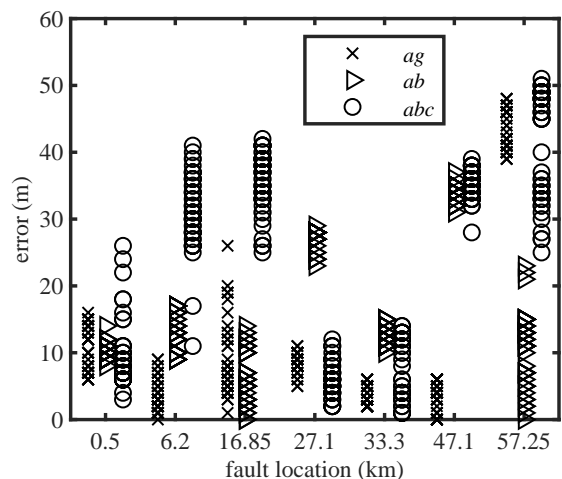


Figure 8: Error in distance estimation for different fault resistance values

4.3 Effect of Noise and Harmonics

The measured voltages and currents are susceptible to perturbations e.g. electromagnetic interference (noise) and the accuracy of the measuring instruments. Gaussian noise is used to add random noise to the measured signals. Two different noise levels have been applied (1% and 2%). The noise level is calculated as a percentage value of the corresponding phase voltage and current values. Fifth and seventh harmonics have been added to the main substation voltage source with values of 1% and 0.5% (referred to the fundamental voltage) respectively to represent a real power system. Faults of different types with a resistance of 10 Ω were simulated and the results are presented in Table 2 showing an accurate estimation for different fault cases.

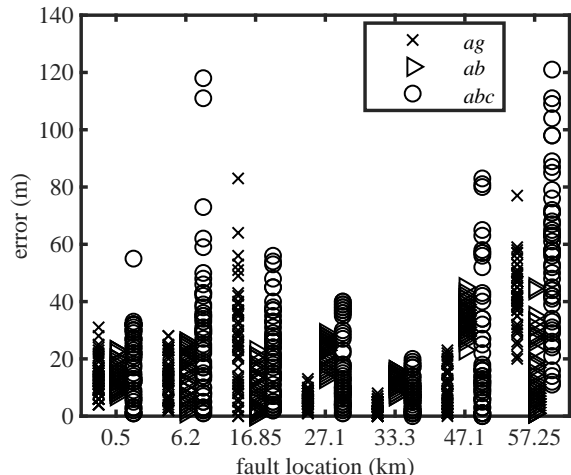


Figure 9: Error in distance estimation for different fault inception angles

Table 2: Error (m) for noise and harmonics test

location (km)	1% noise level			2% noise level		
	<i>ag</i>	<i>ab</i>	<i>abc</i>	<i>ag</i>	<i>ab</i>	<i>abc</i>
0.5	1	24	28	4	5	26
6.2	18	32	32	8	13	57
16.85	43	20	52	17	23	48
27.1	8	22	12	9	26	3
33.3	3	14	7	12	16	14
47.1	10	35	32	29	15	30
57.25	46	7	36	51	9	41

4.4 Effect of Load Variation

The proposed scheme, as well as other impedance based techniques, depend on understanding the load configuration of the system. However, for distribution systems, loads are time varying and it might be impossible to define the exact loading value for different loads without direct measurement at each load point: this is impractical in many applications. To check the effect of load uncertainty on the proposed scheme, it has been tested for three different loading cases.

- case 1: the loads were randomly changed between 50% and normal rated load (100%) to simulate working at medium to normal load condition.
- case 2: the loads were changed between 100% and %125 of the rated load to simulate operation at overload condition.
- case 3: the loads were changed between 50% and %125 to allow some loads to operate below the rated value while others run at overload condition.

For each of these cases, the load scaling factor is different for different loads and is randomly generated. Even though the loads have been varied in the simulation, the fault location process is performed assuming

all loads operate at the rated level e.g. the fault location scheme ignores this variation in the loading. The three fault types used in the previous tests were simulated at different points with a resistance of 10Ω and inception angle of 90° . The error in distance estimation for the three loading cases is shown in Figure 10. An increase in the error is expected in this test because the load variation is ignored. For the simulated fault cases, 82.5% of the points have an error of less than 200 m and more than half of the cases still could be estimated with an error of less than 100 m. The proposed scheme provides acceptable accuracy even without compensating for the load uncertainty.

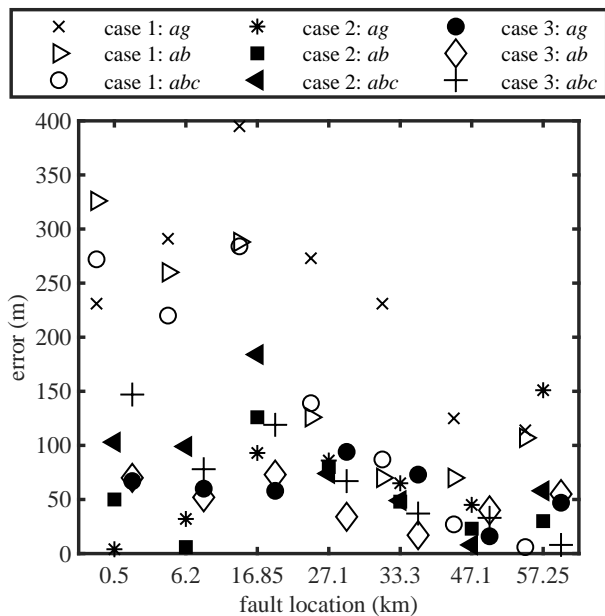


Figure 10: Error in distance estimation for different loading cases

4.5 Comparison with Other Impedance Based Methods

The proposed method has been compared to other impedance based fault location techniques for distribution systems that use synchronized measurements from all generation nodes [5]–[7]. The IEEE 34-bus feeder, which is used in this paper, was used as a case study in [5]–[7]. The comparison considers the effect of the fault resistance with single line to ground (*ag*), phase to phase (*ab*) and three-phase (*abc*) faults at normal loading condition as they are covered by all the methods. The percentage error reported in [5], [6] has been converted to metres using a total feeder length of 58 km. It was not possible to calculate an average error value for phase to phase and three-phase faults in [6] as only the limits of the error variation were mentioned. The

maximum fault resistance values in [5], [6] and [7] are 25, 40 and 100 Ω respectively.

Table 3 summarizes the average (avg) and maximum (max) error reported in these different references and also obtained by the proposed method. Even though the performance of the proposed method is close to that for the methods in [5], [7], the proposed method does not require synchronized measurements from all the generation nodes. The high error in [6] may be attributed to using a short line model to derive the method e.g. ignoring the line capacitance.

Table 3: Error (m) for comparison between methods

method	<i>ag</i>		<i>ab</i>		<i>abc</i>	
	avg	max	avg	max	avg	max
[5]	29	58	29	52	6	12
[6]	272	580	—	1740	—	174
[7]	17	32	15	25	5	7
proposed	11.7	48	16.3	37	23.7	51

4.6 Non-synchronized Measurements

Applying a double end fault location method requires synchronized measurements. Even though the proposed method does not require synchronized measurements from all the generation nodes, the synchronization between the measurements may be totally lost. It will not be possible to apply the proposed method directly. Solving for the synchronization error before using non-synchronized measurements has been reported in [23], [24]. A different proposal is presented in this paper using a single end fault location method. The challenge with the single end methods based on the system fundamental frequency analysis is the representation of the DGs. In [25], the authors presented a new single end wideband fault location method for distribution systems without distributed generation. The method in [25] uses the fault generated transient to estimate the fault distance similar to the double end method proposed in this paper. The theory and operation of the single end method are not described in this paper to save space and are available in [25]. The measurements at all the DGs (as discussed in this paper) are used to provide an estimate for the DG impedance in the high frequency range required by the fault location method. Therefore, the proposed method in [25] accompanied with the high frequency impedance of the DGs estimated using the non-synchronized measurements can be used to locate faults in distribution systems with DGs using non-synchronized measurements. This single end method can be used as an alternative/backup to the proposed double end method and is employed when the synchronization between the measurements is lost.

Faults of different types with a resistance of 10 Ω have been simulated at different locations. The measurements at the three DGs in the system considered have been used to estimate the DG impedance in the high frequency range. The single end method has been applied using the measurements at the main substation and the results are shown in Figure 11. It is clear that the accuracy of the single end method is lower than that obtained in the previous results using the double end method. However, the error value for all cases is less than 200 m. For the system considered with a main feeder length of 58 km, this level of error is low.

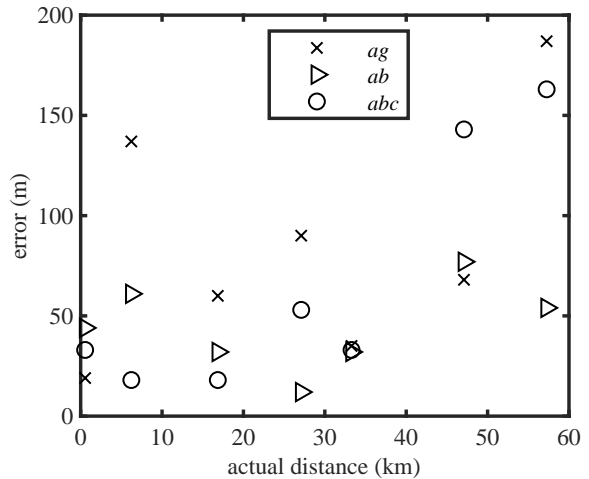


Figure 11: Error in distance estimation using non-synchronized measurements

5 Conclusions

A wideband fault location scheme for distribution systems in the presence distributed generation of different types has been presented and evaluated in this paper. The proposed scheme analyses the system using the high frequency non-fundamental components calculated from the available synchronized and non-synchronized measurements. DGs with non-synchronized measurements have been represented by an equivalent impedance over the high frequency range of interest. The proposed method is applicable to unbalanced distribution systems and also valid for untransposed lines. The IEEE 34-bus feeder that contains unbalanced loads and asymmetrical line configurations has been used to evaluate the method. The evaluation scenarios considered the effect of fault type, fault point, fault resistance, inception angle, noise in measurements and load uncertainty. Even though the loads were considered time varying in the simulation, the fault location algorithm ignored this variation.

The total number of fault cases simulated at different scenarios was 2205. The proposed method es-

estimated 2177 cases (98.7%) with an error in distance estimation of less than 100 m. Note that the length of the longest path in the simulated distribution feeder is about 58 km. Therefore, this level of accuracy is high and the resolution can be considered as 100 m. The comparison with other methods showed the accuracy of the proposed method without the need for synchronized measurements from all generation nodes. Locating faults along laterals/branches is an interesting point for future work.

References

- [1] S. S. Kaddah, M. M. El-Saadawi, and D. M. El-Hassanin, "Influence of distributed generation on distribution networks during faults," *Electric Power Components and Systems*, vol. 43, no. 16, pp. 1781–1792, 2015.
- [2] The Intergovernmental Panel on Climate Change, *Special report on renewable energy sources and climate change mitigation*. [Online]. Available: <http://www.ipcc.ch/report/srren/>.
- [3] M. Shafiullah and M. A. Abido, "A review on distribution grid fault location techniques," *Electric Power Components and Systems*, vol. 45, no. 8, pp. 807–824, 2017.
- [4] A. Kamel, M. A. Alaam, A. M. Azmy, and A. Y. Abdelaziz, "Protection coordination for distribution systems in presence of distributed generators," *Electric Power Components and Systems*, vol. 41, no. 15, pp. 1555–1566, 2013.
- [5] S. F. Alwash, V. K. Ramachandaramurthy, and N. Mithulananthan, "Fault-location scheme for power distribution system with distributed generation," *IEEE Transactions on Power Delivery*, vol. 30, no. 3, pp. 1187–1195, 2015.
- [6] J. J. Mora-Florez, R. A. Herrera-Orozco, and A. F. Bedoya-Cadena, "Fault location considering load uncertainty and distributed generation in power distribution systems," *IET Generation, Transmission & Distribution*, vol. 9, no. 3, pp. 287–295, 2015.
- [7] C. Orozco-Henao, A. S. Bretas, R. Chouhy-Leborgne, A. R. Herrera-Orozco, and J. Marín-Quintero, "Active distribution network fault location methodology: A minimum fault reactance and Fibonacci search approach," *International Journal of Electrical Power & Energy Systems*, vol. 84, pp. 232–241, 2017.
- [8] A. Bahmanyar and S. Jamali, "Fault location in active distribution networks using non-synchronized measurements," *International Journal of Electrical Power & Energy Systems*, vol. 93, pp. 451–458, 2017.
- [9] C. Orozco-Henao, A. S. Bretas, A. R. Herrera-Orozco, J. D. Pulgarín-Rivera, S. Dhulipala, and S. Wang, "Towards active distribution networks fault location: Contributions considering DER analytical models and local measurements," *International Journal of Electrical Power & Energy Systems*, vol. 99, pp. 454–464, 2018.
- [10] F. M. Abo-Shady, M. A. Alaam, and A. M. Azmy, "Impedance-based fault location technique for distribution systems in presence of distributed generation," in *IEEE International Conference on Smart Energy Grid Engineering (SEGE)*, 2013, pp. 1–6.
- [11] R. Dashti and J. Sadeh, "Applying dynamic load estimation and distributed-parameter line model to enhance the accuracy of impedance-based fault-location methods for power distribution networks," *Electric Power Components and Systems*, vol. 41, no. 14, pp. 1334–1362, 2013.
- [12] M. Goudarzi, B. Vahidi, R. Naghizadeh, and S. Hosseinian, "Improved fault location algorithm for radial distribution systems with discrete and continuous wavelet analysis," *International Journal of Electrical Power & Energy Systems*, vol. 67, pp. 423–430, 2015.
- [13] D. W. P. Thomas, R. J. O. Carvalho, and E. T. Pereira, "Fault location in distribution systems based on traveling waves," in *IEEE Bologna Power Tech Conference Proceedings*, 2003.
- [14] M. Al-Shaher, A. S. Saleh, and M. M. Sabry, "Estimation of fault location and fault resistance for single line-to-ground faults in multi-ring distribution network using artificial neural network," *Electric Power Components and Systems*, vol. 37, no. 7, pp. 697–713, 2009.
- [15] J. J. Mora, G. Carrillo, and L. Perez, "Fault location in power distribution systems using ANFIS Nets and current patterns," in *IEEE/PES Transmission & Distribution Conference and Exposition: Latin America*, 2006.
- [16] P.-C. Chen, V. Malbasa, Y. Dong, and M. Kezunovic, "Sensitivity analysis of voltage sag based fault location with distributed generation," *IEEE Transactions on Smart Grid*, vol. 6, no. 4, pp. 2098–2106, 2015.
- [17] F. C. Trindade and W. Freitas, "Low voltage zones to support fault location in distribution systems with smart meters," *IEEE Transactions on Smart Grid*, vol. 8, no. 6, pp. 2765–2774, 2017.
- [18] W. Guo, L. Mu, and X. Zhang, "Fault models of inverter-interfaced distributed generators within a low-voltage microgrid," *IEEE Transactions on Power Delivery*, vol. 32, no. 1, pp. 453–461, 2017.

- [19] “IEEE standard for interconnecting distributed resources with electric power systems,” *IEEE Std 1547-2003*, pp. 1–28, 2003.
- [20] F. M. Aboshady, D. W. P. Thomas, and M. Sumner, “A wideband single end fault location scheme for active untransposed distribution systems,” *IEEE Transactions on Smart Grid (Early Access)*, 2019. DOI: 10.1109/TSG.2019.2947870.
- [21] M. M. Saha, J. J. Izykowski, and E. Rosolowski, *Fault location on power networks*. Springer Science & Business Media, 2009.
- [22] IEEE PES AMPS DSAS Test Feeder Working Group, *34-bus feeder*. [Online]. Available: <http://sites.ieee.org/pes-testfeeders/resources/>.
- [23] R. K. Aggarwal, D. V. Coury, A. T. Johns, and A. Kalam, “A practical approach to accurate fault location on extra high voltage teed feeders,” *IEEE Transactions on Power Delivery*, vol. 8, no. 3, pp. 874–883, 1993.
- [24] S. Hussain and A. Osman, “Fault location scheme for multi-terminal transmission lines using unsynchronized measurements,” *International Journal of Electrical Power & Energy Systems*, vol. 78, pp. 277–284, 2016.
- [25] F. M. Aboshady, D. W. P. Thomas, and Mark Sumner, “A new single end wideband impedance based fault location scheme for distribution systems,” *Electric Power Systems Research*, vol. 173, pp. 263–270, 2019.

6 Appendix

Table 4: Parameters of the IBDG

parameter	value
rated power	250 kVA
DC side voltage	480 V
line to line AC voltage	250 V
inverter switching frequency	3 kHz
inverter side inductance	0.16 mH
grid side inductance	0.04 mH
filter capacitance	212 μ F
filter damping resistance	0.23 Ω